The first high-redshift Changing Look Quasars

Nicholas P. Ross[1]⋆, Matthew Graham[2], K. E. Saavik Ford[3,4,5], Barry McKernan[3,4,5] Daniel Stern[6] and Giorgio Calderone[7]

[1]*Institute for Astronomy, University of Edinburgh, Royal Observatory, Blackford Hill, Edinburgh EH9 3HJ, United Kingdom*
[2]*Cahill Center for Astronomy and Astrophysics, California Institute of Technology, Mail Code 249/17, 1200 E California Blvd, Pasadena CA 91125, USA*
[3]*Department of Science, BMCC, City University of New York, New York, NY 10007, USA*
[4]*Department of Astrophysics, Rose Center for Earth and Space, American Museum of Natural History, Central Park West at 79th Street, NY 10024, USA*
[5]*Graduate Center, City University of New York, 365 5th Avenue, New York, NY 10016, USA*
[6]*Jet Propulsion Laboratory, California Institute of Technology, 4800 Oak Grove Drive, Mail Stop 169-221, Pasadena, CA 91109, USA*
[7]*INAF – Osservatorio Astronomico di Trieste, Via Tiepolo 11, I-34143 Trieste, Italy*

ABSTRACT

We report on three redshift $z > 2$ quasars with dramatic changes in their C IV emission lines, the first "Changing-Look" quasars at high redshift. This is also the first time the changing-look behaviour has been seen in a high-ionization emission line. SDSS J1205+3422, J1638+2827 and J2228+2201 show interesting behaviour in their observed optical light curves, and subsequent spectroscopy shows significant changes in the C IV broad emission line, with both line collapse and emergence being displayed in rest-frame timescales of ~240-1640 days. Where observed, the profile of the Lyα/N v emission complex also changes, and there is tentative evidence for changes in the Mg II line. Although line measurements from the three quasars show large changes in the C IV flux-line width plane, the quasars are not seen to be outliers when considered against the full $z \sim 2$ quasar population in terms of (rest) Equivalent Width and FWHM properties. We put these observations in context with recent "state-change" models, but note that even in their 'low-state', the C IV CLQs are above ~10% in Eddington luminosity.

Key words: accretion, accretion discs – surveys – quasars: general – quasars: individual: J1100-0053

1 INTRODUCTION

Luminous AGN, i.e. quasars, are now seen to significantly vary their energy output on timescales as short as weeks to months. This observation, and the subsequent mismatch in the expected "viscous" timescale, which for a 10^7 M$_\odot$ central supermassive black hole (SMBH) is ~hundreds of years, was noted over 30 years ago (e.g. Alloin et al. 1985). However, with new photometric light-curve and repeat spectroscopic data, the desire for a deeper understanding of AGN accretion disk physics has recently re-invigorated the field (e.g. Antonucci 2018; Lawrence 2018; Ross et al. 2018; Stern et al. 2018).

The optical continuum variability of quasars has been recognized since their first optical identification (e.g., Matthews & Sandage 1963; MacLeod et al. 2012). Dramatic changes in the broad emission lines (BELs) of quasars has only recently been identified (e.g., LaMassa et al. 2015). Samples of over 100 "Changing Look" quasars (CLQs) or "Changing State" quasars (CSQs) have now been assembled (e.g. MacLeod et al. 2019; Graham et al. 2019a). The community uses both these terms as a cover for the underlying

physics. For sake of argument, CLQs can potentially be thought of as the extension to the BELs of quasar continuum variability (e.g., MacLeod et al. 2012) whereas the CSQs have a 'state-transition' similar to that in Galactic X-ray binaries (Noda & Done 2018; Ruan et al. 2019). In this paper, we use the term 'Changing Look', as we are currently agnostic, and confessedly ignorant, to the underlying physical processes.

CLQs to date have primarily been defined according to the (recombination) Balmer emission line properties with particular attention paid to the Hβ emission line, observed from optical spectroscopy. Recent work report on discoveries of Mg II Changing-look AGN (Guo et al. 2019; Homan et al. 2019). However, current CLQ studies have primarily been at redshifts $z < 1$.

While there have been many studies on triply ionized carbon, i.e C IV, these have tended to focus on broad absorption line quasars (BAL QSOs; see Table 1 of Hemler et al. 2019) or the Baldwin Effect (BEff; Baldwin 1977; Bian et al. 2012; Jensen et al. 2016; Hamann et al. 2017)[1]. Dramatic changes in the collisionally excited

---

⋆ E-mail: npross@roe.ac.uk

[1] As noted in Rakić et al. (2017), two different types of Baldwin effect are present in the literature: the *global* (or *ensemble*) Baldwin Effect, which

Line	λ / Å	Transition energy / eV	Ionization energy / eV	Transition Levels Lower			Upper			Wavenumber / cm^{-1}	$A_{i,j}$ ($\times10^8$ / s^{-1})
H LyLim	912.324	13.5984	13.5984	$1s$	^{2}S	1/2	∞			109 678.7	1.23×10^{-6}
H Lyα	1215.670	10.1988	13.5984	$1s$	^{2}S	1/2	2			82 259.2	4.67
N v	1238.821	10.0082	97.8901	$1s^22s$	^{2}S	1/2	$1s^22p$	^{2}P$^{\text{o}}$	3/2	80 721.9	3.40
N v	1242.804	9.9762	97.8901	$1s^22s$	^{2}S	1/2	$1s^22p$	^{2}P$^{\text{o}}$	1/2	80 463.2	3.37
C iv	1548.187	8.0083	64.4935	$1s^22s$	^{2}S	1/2	$1s^22p$	^{2}P$^{\text{o}}$	3/2	64 591.7	2.65
C iv	1550.772	7.9950	64.4935	$1s^22s$	^{2}S	1/2	$1s^22p$	^{2}P$^{\text{o}}$	1/2	64 484.0	2.64
[He ii]	1640.474	7.5578	54.4178	$2p$	^{2}P$^{\text{o}}$	3/2	$3d$	^{2}D	5/2	60 958.0	10.35
[He ii]	1640.490	7.5578	54.4178	$2p$	^{2}P$^{\text{o}}$	3/2	$3d$	^{2}D	3/2	60 957.4	1.73
C iii]	1906.683	6.5026	47.8878	$1s^22s^2$	^{1}S	0	$1s^22s2p$	^{3}P$^{\text{o}}$	2	52 447.1	5.19×10^{-11}
C iii]	1908.734	6.4956	47.8878	$1s^22s^2$	^{1}S	0	$1s^22s2p$	^{3}P$^{\text{o}}$	1	52 390.8	1.14×10^{-6}
Mg ii	2795.528	4.4338	15.0353	$2p^63s$	^{2}S	1/2	$2p^63p$	^{2}P$^{\text{o}}$	3/2	35 760.9	2.60
Mg ii	2802.705	4.4224	15.0353	$2p^63s$	^{2}S	1/2	$2p^63p$	^{2}P$^{\text{o}}$	1/2	35 669.3	2.57
H Ba β	4861.333	2.5497	13.5984	2			4			20 564.8	0.0842

Table 1. Strong UV/optical spectral emission lines in quasars, and their atomic data. Data from the NIST Atomic Spectra Database (Kramida et al. 2018; Kramida et al. 2019). The Transition Energies are $E = hc/\lambda$ for the given wavelength. The Ionization Energy is the energy required to ionize the given species, e.g. 64.49 eV are needed to create a C v ion. Transitions Level configurations are given in standard spectroscopic notation $A_{i,j}$ are transition probabilities. Data from the NIST Atomic Spectra Database (Kramida et al. 2018; Kramida et al. 2019).

broad *emission* line (BEL) of C iv and indeed C iii] have not to this point been reported.

Here, we present new results for three quasars which show dramatic changes in their C iv and C iii] broad emission line properties as well as in their underlying continuum. These are some of the first examples of "Changing Look Quasars" at high ($z > 1$) redshift. Moreover, these are the first cases for substantial changes of ions with high ionization potentials (I.P.'s >2 Rydberg), thus linking the ionizing photons to the energetic inner accretion disk, potentially by inverse Compton scattering of lower energy photons to higher energies.

Details of the atomic transitions that produce strong rest-frame UV/optical lines in quasars are given in Table 1. In this paper we use the wavelengths of 1548.202 and 1550.774 Å for the C iv doublet (Kramida et al. 2018). For ionisation energies, 47.89 eV (3.519 Ry) is required for doubly-ionised C III to become triply-ionised C iv. 64.49 eV (4.74 Ry) is the energy needed to ionize C iv itself. This energy corresponds to a thermal temperature of $T \gtrsim 4\times10^5$, implying a heating energy source of (soft) X-ray photons ($k_B = 8.617\times10^{-5}$ eV /K).

Wilhite et al. (2006) examine C iv variability in a sample of 105 quasars observed at multiple epochs by the Sloan Digital Sky Survey (SDSS; York et al. 2000; Stoughton et al. 2002; Abazajian et al. 2009a). They find a strong correlation between the change in the C iv line flux and the change in the line width, but no correlations between the change in flux and changes in line center and skewness. These authors find that the relation between line flux change and line width change is consistent with a model in which a broad line base varies with greater amplitude than the line core. The C iv lines in these high-luminosity quasars appear to be less responsive to continuum variations than those in lower luminosity AGN.

Richards et al. (2011) explored the BEL region in over 30,000 $z > 1.54$ SDSS quasars, concentrating on the properties of the C iv emission line. These authors consider two well-known effects involving the C iv emission line: *(i)* the anti-correlation between the

is an anti-correlation between the Equivalent Width (EW) of the emission line and the underlying continuum luminosity of *single-epoch* observations of a *large number* of AGN and second, the *intrinsic* Baldwin effect, the same anti-correlation but in an *individual, variable* AGN (Pogge & Peterson 1992).

C iv equivalent widths (EWs) and luminosity (i.e., the Baldwin Effect; BEff) and *(ii)* the blueshifting of the peak of C iv emission with respect to the systemic redshift. We denote the velocity offset of emission lines as V_{off} and use the convention that a positive V_{off} value means the line is blueshifted while a negative V_{off} value means the line is redshifted. Richards et al. (2011) find the blueshift of the C iv emission line, is found to be nearly ubiquitous, with a mean shift of V_{off} ~810 km s^{-1} for radio-quiet (RQ) quasars and V_{off} ~360 km s^{-1} for radio-loud (RL) objects. Richards et al. (2011) also find the BEff is present in both the RQ and RL studied samples. These author conclude that these two C iv parameters (EQW and blueshift) are capturing an important trade-off between "disk" and "wind" components in the disk-wind model of accretion disks (e.g., Murray et al. 1995; Elvis 2000; Proga et al. 2000; Leighly 2004), with one dominating over the other depending on the shape of the SED.

Using the multi-epoch spectra of 362 quasars from the Sloan Digital Sky Survey Reverberation Mapping (SDSS-RM; Shen et al. 2015, 2019) project, Sun et al. (2018) investigate the blueshift of C iv emission relative to Mg ii emission, and its dependence on quasar properties. These authors confirm that high-blueshift sources tend to have low C iv EWs, and that the low-EW sources span a range of blueshift. Other high-ionization lines, such as [He ii] , also show similar blueshift properties. The ratio of the line width of C iv to that of Mg ii increases with blueshift. Sun et al. (2018) also find that quasar variability might slightly enhance the connection between the C iv blueshift and EW, though further investigation here is warranted. There is also the finding that the objects with that largest blueshifts are less variable and tend to have higher Eddington ratios. Sun et al. (2018) explain their results these by suggesting that quasar SEDs become *softer* with *increasing Eddington ratio* along with the presence of X-ray shielding by the inner accretion disk. However, a high Eddington ratio alone might be an insufficient condition for the C iv blueshift. Recent investigations also include Meyer et al. (2019) and Doan et al. (2019). Dyer et al. (2019) provide a detailed analysis of 340 quasars at high-redshift ($1.62 < z < 3.30$) from the SDSS-RM project, which we will compare our results to.

The purpose of this paper is, for the first time, to systematically access and report on the CLQ phenomenon at high ($z > 2$) redshift. While accessing this phenomenon at an earlier cosmic epoch is somewhat interesting, the main value of this study is we move from

Object	Redshift	g-band (mag)	MJD	Instrument	Exposure Time (seconds)	SDSS Plate-FiberID	Notes
J120544.7+342252.4	2.068	18.27	53498	SDSS	8057	2089-427	
	2.071		58538	DBSP	1800	—	Average conditions
	2.071		58693	DBSP	2400	—	
J163852.9+282707.7	2.185	19.77	54553	SDSS	4801	2948-614	
	2.186		55832	BOSS	3600	5201-178	
	2.182		58583	LRIS	1800	—	
J222818.7+220102.9	2.217	19.97	56189	BOSS	2700	6118-720	
	2.222		56960	BOSS	4500	7582-790	eBOSS reobservation
	2.222		58693	DBSP	2400	—	

Table 2. Details of our spectroscopic observations. Redshift errors are typically ±0.002. Exposure times are from the `plate.fits` file. SDSS, BOSS and eBOSS spectra have $\mathcal{R} \sim 2,000$. DBSP: Double Spectrograph on the Palomar 200-inch telescope. LRIS: Low Resolution Imaging Spectrometer on Keck I 10m telescope.

the low-ionization energy Balmer emission line series to the high-ionization emission lines, in particular C IV $\lambda 1549$.

This paper is organised as follows. In Section 2, we describe our sample selection, catalogues, and observational data sets. In Section 3, we show the high-z quasars and report the line properties for the quasars at the observed epochs. We give a very brief theoretical discussion in Section 4. We present our conclusions in Section 5. We report all magnitudes on the AB zero-point system (Oke & Gunn 1983; Fukugita et al. 1996) unless otherwise stated. For the WISE bands, $m_{AB} = m_{Vega} + m$ where $m = (2.699, 3.339)$ for WISE W1 at 3.4μm and WISE W2 at 4.6μm, respectively (Cutri et al. 2011). We adopt a flat ΛCDM cosmology with $\Omega_\Lambda = 0.73$, $\Omega_M = 0.27$, and $h = 0.71$ in order to be consistent with Hamann et al. (2017). As a guide this cosmology has a $z = 2.000$ comoving radial distance of 5244.3 Mpc, a $\sim 1.25\%$ difference compared to 5179.0 Mpc from $\Omega_\Lambda = 0.70$, $\Omega_M = 0.30$, and $h = 0.70$ that is used in Shen et al. (2011).

2 DATA, CLQ SELECTION AND LINE MEASUREMENTS

In this section we present the photometric data used to select the CLQs, and then give details to the multiwavelength data where we have it, obtained spectroscopy and emission lines measurements.

2.1 Photometry

2.1.1 Optical Photometry

We use optical data from the Catalina Real-time Transient Survey (CRTS; Drake et al. 2009; Mahabal et al. 2011), the Panoramic Survey Telescope and Rapid Response System (PanSTARRS; Kaiser et al. 2010; Stubbs et al. 2010; Tonry et al. 2012; Magnier et al. 2013) and the Zwicky Transient Facility (ZTF; Bellm et al. 2019a).

The CRTS archive[2] contains the Catalina Sky Survey data streams from three telescopes – the 0.7 m Catalina Sky Survey (CSS) Schmidt and 1.5 m Mount Lemmon Survey (MLS) telescopes in Arizona and the 0.5 m Siding Springs Survey (SSS) Schmidt in Australia. CRTS covers up to ~ 2500 deg^2 per night, with 4 exposures per visit, separated by 10 min. The survey observes over 21 nights per lunation. The data are broadly calibrated to Johnson

V (see Drake et al. 2013, for details) and the current CRTS data set contains time series for approximately 400 million sources to $V \sim 20$ above Dec > -30 from 2003 to 2016 May (observed with CSS and MLS) and 100 million sources to $V \sim 19$ in the southern sky from 2005 to 2013 (from SSS). CRTS has been used to study distant quasars previously (Graham et al. 2014, 2015a,b, 2017, 2019a).

PanSTARRS data is obtained via the Pan-STARRS Catalog Search interface[3]. We query the PS1 DR2 Detection catalog.

The ZTF is a new robotic time-domain sky survey capable of visiting the entire visible sky north of -30 deg. declination every night. ZTF observes the sky in the g, r, and i-bands at different cadences depending on the scientific program and sky region (Bellm et al. 2019b; Graham et al. 2019b). The ZTF 576 megapixel camera with a 47 deg^2 field of view, installed on the Samuel Oschin 48-inch Schmidt Telescope, can scan more than 3750 deg^2 per hour, to a 5σ detection limit of 20.7 mag in the r-band with a 30sec exposure during new moon (Masci et al. 2019).

2.2 CLQ Selection

Our high-z CLQs were identified as follows. We selected all 64,774 SDSS DR15 sources with $z > 0.35$ classified as 'QSO', having at least two spectra separated by at least 100 days, and with a corresponding CRTS light curve. We fitted a damped random walk to the CRTS data via Gaussian process regression and the photometric magnitudes at the epochs of the SDSS spectra for a given source are predicted. Those where $|\Delta V| > 0.3$ are then selected for visual inspection. Only three quasars SDSS J120544.7+342252.4 (hereafter J1205+3422), SDSS J163852.93+282707.7 (hereafter J1638+2827) and SDSS J222818.76+220102.9 (hereafter J2228+2201), satisfied these selection criteria and showed interesting or dramatic emission line behaviour.

2.3 Spectra

An overview of our spectroscopic observations is given in Table 2. The spectra are from the SDSS (Stoughton et al. 2002; Abazajian et al. 2009b; Schneider et al. 2010), the SDSS-III Baryon Oscillation Spectroscopic Survey (BOSS Eisenstein et al. 2011; Dawson et al. 2013; Smee et al. 2013; Alam et al. 2015; Pâris et al. 2017)
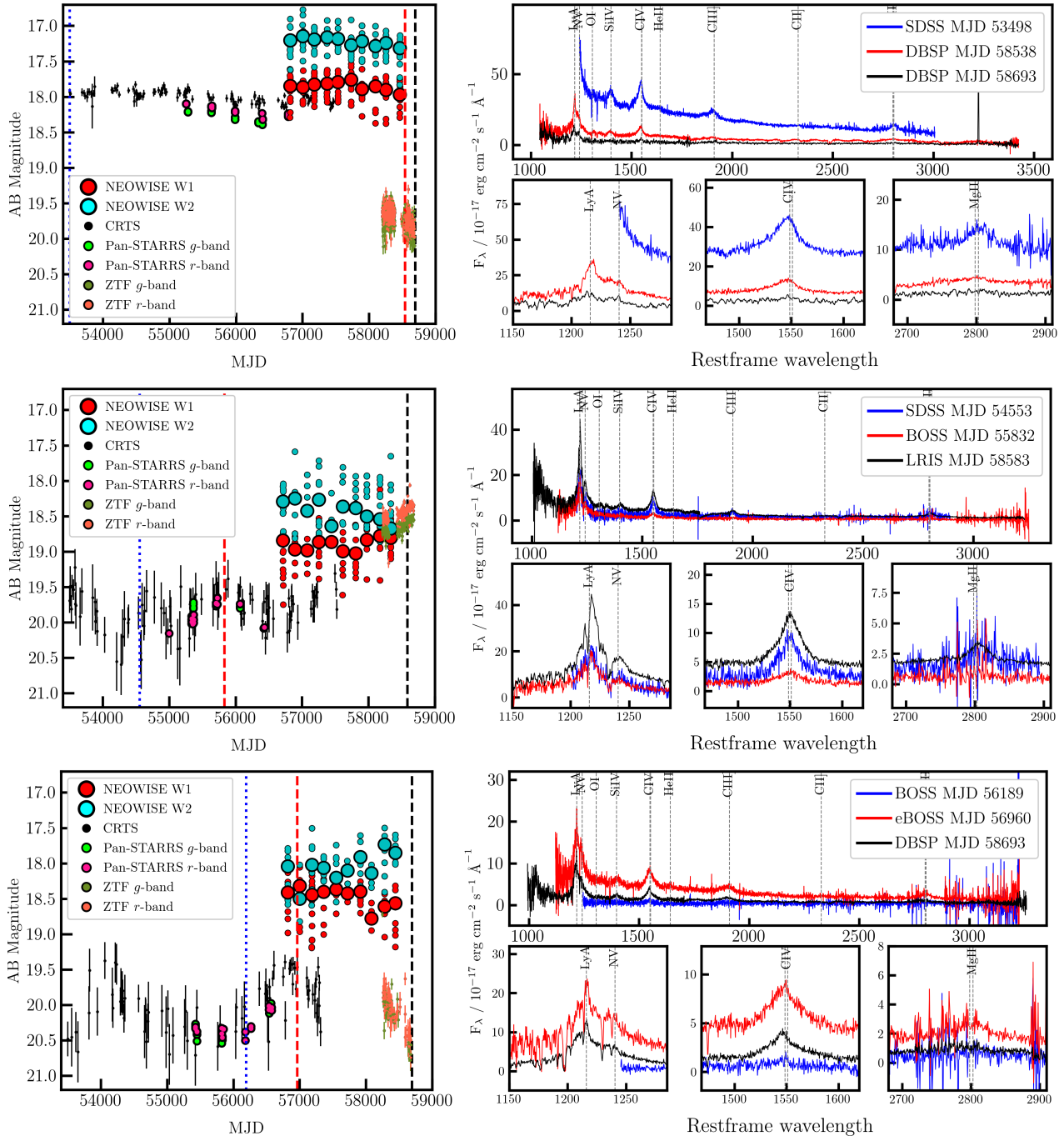
---

[2] http://catalinadata.org

[3] https://catalogs.mast.stsci.edu/panstarrs/

Figure 1. The threes high-z CLQ quasars; SDSS J1205+3422 (top), SDSS J1638+2827 (middle), SDSS J2228+2201 (bottom). The light curve data is present in the panels on the left hand side, with the spectral epoch observational timings given by the vertical lines. The spectra are on the right hand side, with zoom-in's on the Lyα-N v complex, the C iv line and the Mg ii line.

and the SDSS-IV Extended Baryon Oscillation Spectroscopic Survey (eBOSS; Dawson et al. 2016; Abolfathi et al. 2018; Pâris et al. 2018). These quasars were targetted via a range of techniques and algorithms (see Richards et al. 2002; Ross et al. 2012; Myers et al. 2015). The SDSS, BOSS and eBOSS data are supplemented by spectra from the Low Resolution Imaging Spectrometer (LRIS) on the 10m Keck I telescope (Oke et al. 1995). and the Double Spectrograph (DBSP) instrument on the Palomar *Hale* 5m telescope.

2.4 Emission Line and Power-law slope measurements

We use the measured quasar emission line properties from several catalogues: Shen et al. (2011), Hamann et al. (2017), Kozłowski (2017) and Calderone et al. (2017).

Shen et al. (2011) present a compilation of properties of the 105,783 quasars in the SDSS Data Release 7 (DR7) quasar catalog (DR7Q; Schneider et al. 2007). Shen et al. (2011) report non-zero C iv FWHM and EWs for approximately half (51,501) of the full DR7Q, and non-zero Mg ii FWHM and EWs for 80% (84,183) of the DR7Q quasars). Measured line values using the methods and

catalogue from Shen et al. (2011). $M_I(z = 2)$ is the Absolute *i*-band magnitude *K*-corrected to $z = 2$; Bolometric luminosity computed from the monochromatic luminosity at 1350Å using the spectral fits and bolometric corrections (BC = 3.81) in Richards et al. (2006); Line luminosity, FWHM, rest-frame equivalent width, and their errors for the whole C IV profile. Power-law slope α_λ for the continuum fit for C IV; Virial BH masses using calibrations of Vestergaard & Peterson (2006). Eddington ratio computed using the virial BH mass.

Calderone et al. (2017) present the Quasar Spectral Fitting (QSFIT) software package which among other quantities provides luminosity estimates as well as width, velocity offset and equivalent width of 20 emission lines, including C IV, C III] and Mg II . We attempt to process and fit all nine spectra using the lastest version (v1.3.0) of the QSFIT online calculator and setting $E(B - V) = 0.00$. The host galaxy and blended iron emission at rest-frame optical wavelengths components are automatically disabled when they can not be constrained by the available data, such as the case for all our objects (we do not have infrared spectral data).

Hamann et al. (2017) investigate in robust detail the UV continuum and the C IV (and N V λ1238, 1242 Å) emission lines for over 200,000 quasars in BOSS DR12Q (Pâris et al. 2017). The quasar redshift are limited to the range $1.53 \le z \le 5.0$ so that C IV and the adjacent continuum are covered by BOSS. These measurements provide line profile information and flux ratios[4] Hamann et al. (2017) was focused on $z \ge 2$ quasars and specifcally their C IVproperties in order to understand the high-*z* "Extremely Red Quasar" population Ross et al. (2015); Zakamska et al. (2016); Perrotta et al. (2019); Zakamska et al. (2019). As such, we prefer the Hamann et al. (2017) emission line values where available, though this is only for two out of our nine spectra.

When using the Shen et al. (2011) catalogue, we report line luminosity, FWHM, rest-frame equivalent width, and their errors for the whole Mg II profile (this catalogue also quotes values for just the broad Mg II component, but the differences for our objects is negligible). The line luminosities in Calderone et al. (2017) are given in units of 10^{42} erg s^{-1}, while the line luminosities in Shen et al. (2011) are in units of $\log(L)$. We do not report the Shen et al. (2011) error on the line luminosity.

Power-law continuum slopes, α, where $f_\lambda \propto \lambda^\alpha$, are also reported in these catalogues and from QSFit. We quote the most appropriate value given the emission line wavelength.

2.5 Multi-wavelength properties

Mid-infrared data (3.4 and 4.6μm) is available from the beginning of the Wide-field Infrared Survey Explorer (WISE) mission (2010 January; Wright et al. 2010) through the fifth-year of NEOWISE-R operations (2018 December; Mainzer et al. 2011). The WISE scan pattern leads to coverage of the full-sky approximately once every six months (a "sky pass"), but the satellite was placed in hibernation in 2011 February and then reactivated in 2013 October. Hence, our light curves have a cadence of 6 months with a 32 month sampling gap.

3 RESULTS

3.1 Overall Spectral Evolution

Figure 1 presents the optical and infrared light curves for three high-*z* CLQ quasars. Figure 1 also shows the spectra for each epoch, with the MJD of observation given by the dashed vertical lines in the light curves.

For J1205+3422, our spectral observations cover 5195 days observed, 1691 days in the rest-frame. For J1205+3422 is identified in SDSS as a bright $g \approx 18.0$, blue-sloped quasar with broad Si IV , C IV, C III] and Mg II observed in the initial spectrum (MJD 53498; 2005-May-08). C III] and C IV are seen to have large blueshifts of $\approx$2600±150 and $\approx$1150±100 km s^{-1}, respectively. By the time the 2019 spectra were taken (MJD 58538, 2019-Feb-24 and MJD 58693 2019-Jul-29), however, the light curve has dropped by $\sim$1.5 magnitudes and the spectra are significantly less steep. While Lyα and N V are detectable in both the MJD 58538 and MJD 58693 DBSP spectra, C IV has all but disappeared in the MJD 58693 spectrum. The broad C III] emission has disappeared between the 2005 and 2019 spectra. *The changes in C IV and C III] going from broad emission to barely detectable have on the timescales of $\approx$50 days in the rest-frame.*

For J1638+2827, our spectral observations cover 4030 days observed, 1265 days in the rest-frame. Here, in the initial epoch spectrum, C IV is broad and bright, as is C III] . However, just over 400 days in the rest-frame later, the broad C IV and C III] BEL have to faded, the continuum slope around 1400Å has changed from $\approx$-1.48 to $\approx$-2.25, but the Lyα /N V emission complex is very similar in shape and line flux intensity. Around 870 days in the rest-frame after the second spectral epoch, Lyα , N V , C IV, C III] and Mg II are all apparent and broad, with Mg II being seen for the first time at high signal-to-noise. The light curve is consistent with this spectral brightening, increasing from around $\sim$19.5-20.5th magnitude to $\sim$18.5 in the optical band. An absorption feature between Lyα and N V is seen in all three spectral epochs.

For J2228+2201, our spectral observations cover 2504 days observed, 778 days in the rest-frame. Over the course of 240 days in the rest-frame, C IV and C III] both *emerge* as BELs and the standard UV/blue continuum slope increases in flux. Then, over the course of 538 days in the rest-frame, the broadline emission, while still very present, reduces in line flux the UV/blue continuum diminishes, though is still more luminous than the initial BOSS spectrum.

3.2 Emission line evolution

Emission line measurements from the catalogues of Shen et al. (2011). Hamann et al. (2017), Kozłowski (2017) or the QSFit routine of Calderone et al. (2017) are presented in Table **??**.

From Figure 2 there appears to be a strong correlation between the change in the line flux and the change in the line width. Figure 2 shows the epoch-to-epoch flux ratio versus the ratio of line widths.

For the BOSS spectrum of J2228+2201 on MJD 56189, some of the data are "masked" (i.e. they have and_mask != 0) in the FITS file at wavelengths $\lesssim$1600Å (rest-frame). This typically means there is some potential problem in using those data. However, visual inspection shows strong broad C IV emission, so we disable the check on the mask, and report the line fits in Table 3 and show the C IV line fits in **??**.

---

[4] This emission-line catalog can be downloaded from here.

Object	MJD	line	Line Lumin.	FWHM	V_{off}	E.W.	α_λ
	53498	C IV	511±13	9593±287	1172±74	15.9±0.4	−1.64 ± 0.01
	53498	C III]	441±10	14959±352$^{(b)}$	2616±147	25.10±0.59	−1.65 ± 0.01
	53498	Mg II	327±20	4907±387	−274 ± 419	26.66±1.65	−1.65 ± 0.01
J1205+3422	58538	Lyα	952±1.1	12242±15	−1679 ± 6	165±0.2	—
	58538	C IV	1037±5	>15000	983±40	—	
	58538	C III]	167±0.9	>15000	2734±46	45±0.2	—
	58538	Mg II	216±1.4	13940±94	−465.2 ± 38	88±0.6	—
	58693	Lyα	271±0.9	9637±52	−447 ± 13	85.1±0.3	—
	58693	C IV	52±0.9	5046±26	1053±17	24.0±0.2	—
	58693	C III]	59±0.9	10751±	1097±77	36±0.6	—
	58693	Mg II	69±1.5	14983±346	−190 ± 134	72±1.6	—
	54553	C IV	259±14	4554±378	337±463	32.8±1.7	
(Shen11)	54553	C III]	130±10	3852±402	−236 ± 565	36.7±2.8	−1.47 ± 0.20
	54553	Mg II	139	4757±2224	−944 ± 568	119±40	−1.49 ± 0.54
J1638+2827	55832	Lyα	288±11	4444±243	-463±68	103.69±3.99	
	55832	C IV	61±3	5878±253	277±102	40.0±1.7	-2.25±0.05
	55832	C III]	15±5	11421±3654	>3000	14.8±4.5	-2.25±0.05
	58583	Lyα	785±1	4956±4	−641 ± 2	90±0.1	—
	58583	C IV	311±1	5739±14	−167 ± 6	58±0.1	—
	58583	C III]	52±0.8	3917.4 68.837	1514±127	124±2	—
	58583	Mg II	157±2	10565±129	−450 ± 52	92±1	—
	56189	C IV	32±3.5	7663±881	538±352	50.2±5.6	—
	56189	C III]	34±6	13748±2869	1851±1140	63±12	−0.46 ± 0.21
	56189	Mg II	25±6	7253±1712	−931 ± 708	51±10.95	−0.46 ± 0.21
	56960	Lyα	121±38	3580±673	−16±171	13.52 ±4.21	—
J2228+2201	56960	C IV	229±4	8911±169	92±68	46.8±0.9	—
	56960	C III]	185±5	-	2701±225	47.75±1.29	—
	56960	Mg II	99±4	7312.6±340	188±137	50.75±2.21	—
	58693	Lyα	447±5	8133±93	613±130	56±0.6	—
	58693	C IV	41±1	4914±65	160±27	25±0.3	—
	58693	C III]	107±1.2	>15000	2422±67	—	—
	58693	Mg II	177±1.1	>15000	1000±2617	16±36	—

Table 3. Line Measurement information for the nine epochs for the 3 quasars. Line Luminosity is in units of 10^{42} erg s^{-1}; FWHM and V_{off} in km s^{-1}, where positive values of V_{off} means the line is blueshifted. Equivalent widths are in units of Å . Positive values of V_{off} means the line is blueshifted. All measuremennts are from QSFIT, except for J1638+2827 (MJD 54553) which are from Shen et al. (2011). $^{(d)}$Emission line modelled with two components.
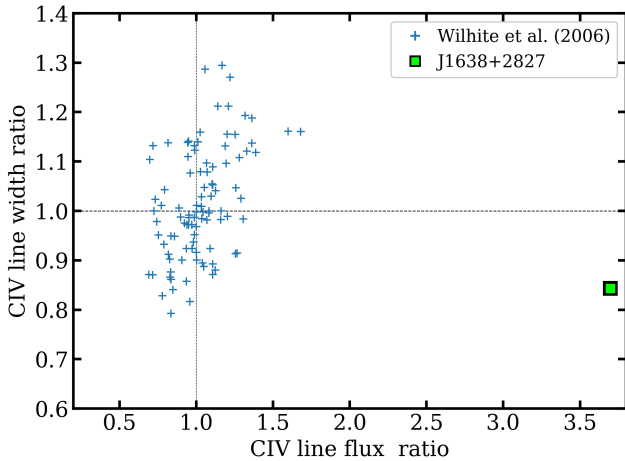

Figure 2. The Change in C IV line width vs. line flux change. We compare our object J1638+2827 with the sample from Wilhite et al. (2006) with a sample of 105 quasars observed at multiple epochs by the SDSS. J1638+2827 is a substantial outlier in this parameter space.

3.3 The C IV **Baldwin Effect**

The Baldwin Effect (Baldwin 1977) is an empirical relation between emission-line REWs and continuum luminosity in quasars (Shields 2007; Hamann et al. 2017; Calderone et al. 2017) There is an anti-
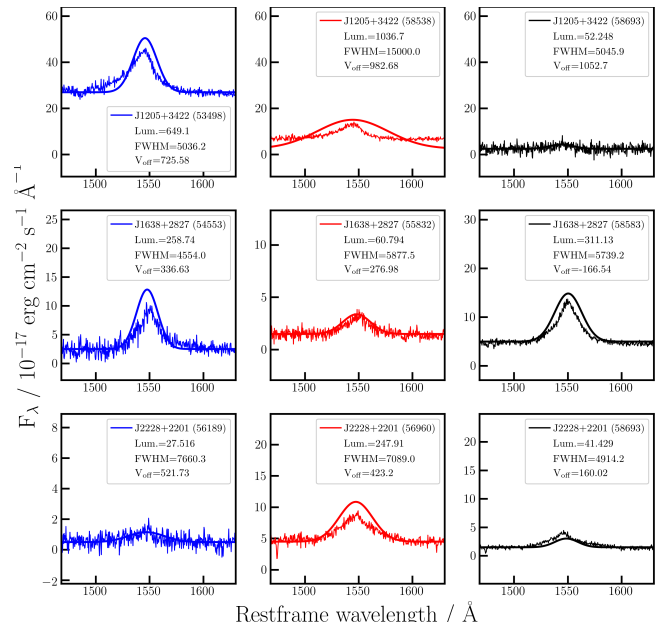

Figure 3. The C IV emission line and the subsequent QSFit model and parameters.

Object	MJD	Cont. Lumin	Cont. slope
	53498	40040±34	-1.656± 0.006
J1205+3422	58538	—	—
	58693	—	—
	54553	3774±111	-1.472±0.197
J1638+2827	55832	2433±14	-2.316±0.051
	58583	3292±9	-0.541±0.010
	56189	—	—
J2228+2201	56960	7889±14	-1.729±0.015
	58693	—	—

Table 4. Quasar continuum νL_ν luminosities and slopes, at the fixed rest-frame wavelengths 1450Å from QSFIT. The luminosities are in units of 10^{42} erg s^{-1}.

correlation between the emission-line REWs and e.g. 1450Å rest continuum luminosity, so that as the underlying UV continuum luminosity increases, the EW decreses, see Figure 5 Our Figure 5 is a reproduction of Figure 15 from Calderone et al. (2017).

The plotted values are `CONT1450__LUM` and `BR_CIV_1549__EW`. `CONT1__LUM` is the νL_ν luminosity at wavelength. This selects 20,374 quasars. The slope β is -0.1997. Checking with Kozłowski (2017), using their bolometric luminosity gives a slope of $\beta = -0.251$, in line with that from Hamann et al. (2017) ($\beta = -0.23$). Lorem ipsum dolor sit amet, consectetur adipiscing elit. Aliquam porta sodales est, vel cursus risus porta non. Vivamus vel pretium velit. Sed fringilla suscipit felis, nec iaculis lacus convallis ac. Fusce pellentesque condimentum dolor, quis vehicula tortor hendrerit sed. Class aptent taciti sociosqu ad litora torquent per conubia nostra, per inceptos himenaeos. Etiam interdum tristique diam eu blandit. Donec in lacinia libero.

Nunc semper quam et leo interdum vulputate eu quis magna. Sed nec arcu at orci egestas convallis. Aenean quam velit, aliquam vitae viverra in, elementum vel elit. Nunc suscipit aliquet sapien a suscipit. Cras nulla ipsum, posuere eu fringilla sit amet, dapibus ultricies nulla. Nullam eu augue id purus mollis dignissim sed et libero. Phasellus eget justo sed neque pellentesque egestas nec id arcu. Donec facilisis pulvinar sapien et fringilla. Suspendisse vestibulum rhoncus sapien id laoreet. Morbi et orci vitae tortor imperdiet imperdiet. In hac habitasse platea dictumst. Vivamus vel neque id mi ultrices tristique. Integer quam libero, ornare vel gravida in, feugiat a ante. Nam dapibus, tellus vitae pellentesque cursus, dui nisl egestas augue, non fermentum nisl est nec nisi. Vestibulum nec mi justo, eget dapibus velit.

4 DISCUSSION

The variable properties of high-z quasars, however, has been less well studied. Reasons for this include more massive systems will tend to have longer timescales with e.g. $t_{\rm dyn} \sim M^2$ if $t_{\rm dyn} = \sqrt{R^3/GM}$ and $R_{\rm Sch} = 2GM/c^2$.

The Balmer series in hydrogen is due to the recombination cascade between different principal quantum numbers n, and the $n = 2$ level (e.g., Seaton 1959a,b). Lower redshift $z < 0.9$ CLQs have traditionally been identified via large changes in the Hβ emission line. Hβ emission is associated with a 2.55 eV energy difference. Thus we can place the high-z, HIL C IV in context of Balmer Hβ CLQs at lower-z.

C IV is one of the strongest collisionally excited lines in quasar spectra Hamann & Ferland (e.g. 1999). The line is most prominent
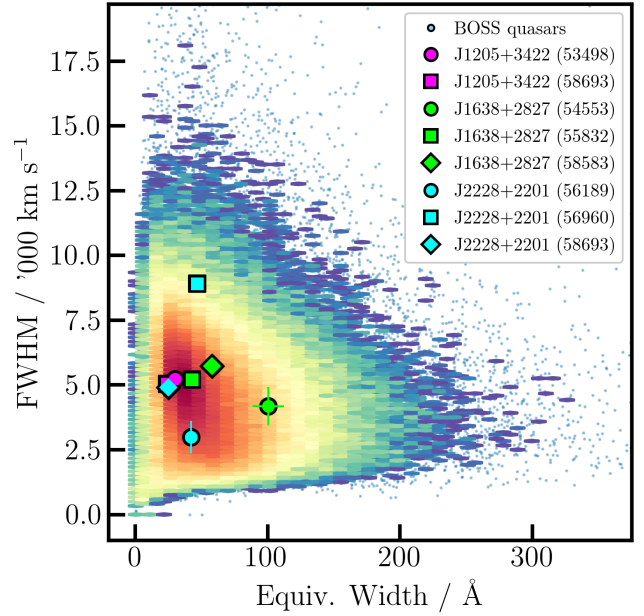

Figure 4. The Rest Equivalent Width (REW) vs. Full Width Half Maximum (FWHM) of the C IV emission line in the BOSS DR12 quasar sample using the catalogue of Hamann et al. (2017).

at n H $\approx$ 1010 cm-3 and log $U \approx$ -1.5, which are the canonical BELR parameters deduced over from early analysis of the C IV emission (Davidson & Netzer 1979). A dimensionless ionization parameter $U \equiv \Phi(H)/cn_H$, where c is the speed of light and n_H is the total hydrogen density (H^0 + H$^+$).

C IV probes the photoionization environment produced by the innermost disk, as indicated by RM time-delay measurements. In standard Shakura & Sunyaev (1973) thin disk models, large changes in the continuum flux are not permitted over short timescales due to the relatively long viscous time associated with such disks. Given the observed short timescale continuum variations, it is not surprising that the Shakura & Sunyaev (1973) disk may fail on other fronts. The C IV variations observed in our sources...

This indicates they may comfortably fit into the sample of CIV variable QSOs explored by Dyer et al. (2019), and similar to those authors we suggest slim accretion disk models e.g., Abramowicz et al. (1988) or inhomogeneous disk models (e.g., Dexter & Agol 2011) may provide viable explanations for our observations. I want to say a bit more here about the generic probe of photoionization vs shielding and conditions in the BL region but that will take more time.

This implies that the variable C IV in our sample arises through different emission mechanisms than is usual for high-z quasar...

4.1 The Baldwin Effect

The variable properties of the rest-frame UV quasar emission lines have been long studied, with the global (or ensemble) Baldwin Effect (the anti-correlation between the EW of the emission line and the underlying continuum luminosity of single-epoch observations of a large number of AGN, first noted in Baldwin (1977). More recently, the intrinsic Baldwin effect, the same anti-correlation but in an individual, variable AGN.

The X-ray Baldwin Effect (e.g., Iwasawa & Taniguchi 1993)... Bachev et al. (2004) find a 10-fold decrease in EW C IV with Ed-

Object	MJD	M_i	L_{bol}	M_{BH}		η_{Edd}		Ref.
				Mg II	C IV	Mg II	C IV	
J1205+3422	53498	-27.74	47.216±0.004	9.55±0.05	9.49±0.04	-0.434	-0.374	Shen11
	58538							
	58693							
J1638+2827	54553	-26.75	46.166±0.04	9.03±0.37	8.74±0.15	-0.964	-0.677	Shen11
	55832	-26.40	46.721±0.073	9.34	9.13	-0.717	-0.509	Kozl17
	58583							
J2228+2201	56189	-25.46	46.231±0.073	9.45	8.73	-1.317	-0.602	Kozl17
	56960							
	58693							

Table 5. Physical properties of the C IV CLQs and M87. $M_I(z = 2)$ is the Absolute i-band magnitude K-corrected to $z = 2$; Bolometric luminosity computed from the monochromatic luminosity at 1350Å using the spectral fits and bolometric corrections (BC = 3.81) in Richards et al. (2006). Virial BH masses using calibrations of Vestergaard & Peterson (2006). η_{Edd} is the base 10 logarithm of the Eddington ratio computed using the virial BH mass. Shen11 is Shen et al. (2011). Kozl17 is Kozłowski (2017).
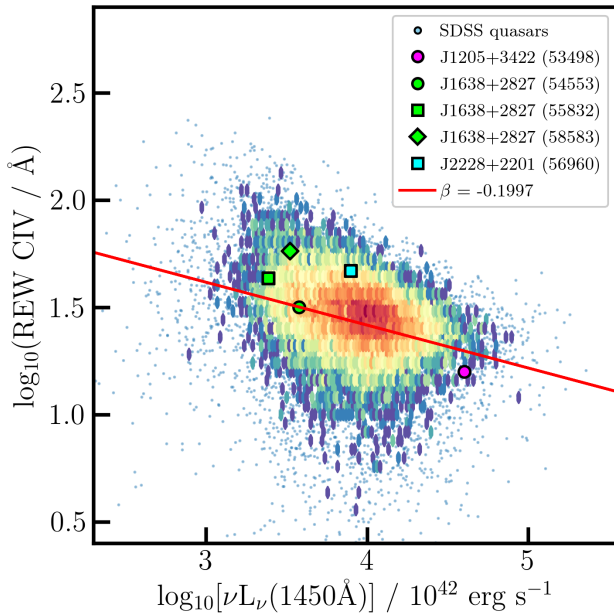
Figure 5. The C IV Equivalent width and the underlying continuum luminosity, commonly referred to as The Baldwin Plot. The continuum luminosities are from Calderone et al. (2017), the REW measurements are Table 4.

dington ratio (decreasing from ~1 to ~0.01), while N V shows no change. These trends suggest a luminosity-independent "Baldwin effect" in which the physical driver may be the Eddington ratio. Ge et al. (2016) Broad emission lines is a prominent property of type I quasi-stellar objects (QSOs).

4.2 Eddington ratios and State Changes

The broad UV and optical lines in quasars are most sensitive to the extreme ultraviolet (EUV) part of the spectral energy distribution (SED), with C IV (and indeed [He II] and N V) being at the higher energy end of the EUV distribution.

The soft X-ray excess – the excess of X-rays below 2 keV with respect to the extrapolation of the hard X-ray spectral continuum model – is a very common feature among type 1 active galactic nuclei (AGN). Noda & Done (2018) note that The soft X-ray excess produces most of the ionizing photons, so its dramatic drop leads to the disappearance of the broad-line region, driving the "changing-

look" phenomena. major difference is that radiation pressure should be much more important in AGNs, so that the sound speed is much faster than expected from the gas temperature. This spectral hardening appears similar to the soft-to-hard state transition in black hole binaries at $L/L_{Edd} \sim 0.02$ (i.e. $\eta_{Edd} \sim -1.7$, where the inner disc evaporates into an advection dominated accretion flow, while the overall drop in luminosity appears consistent with the hydrogen ionization disc instability. Crucially Noda & Done (2018) make the prediction that all changing-look AGNs are similarly associated with the state transition at $L/L_{Edd} \sim$ a few per cent. Jiang et al. (2014, 2016, 2019b). Jiang et al. (2019a) use global three dimensional radiation magneto-hydrodynamic simulations to study the properties of inner regions of accretion disks around a 5×10^8 M$_\odot$ black hole with mass accretion rates reaching 7% and 20% of the Eddington value.

We investigate this reporting the Eddington ratios of the three quasars in Table 5. Lorem ipsum dolor sit amet, consectetur adipiscing elit. Aliquam porta sodales est, vel cursus risus porta non. Vivamus vel pretium velit. Sed fringilla suscipit felis, nec iaculis lacus convallis ac. Fusce pellentesque condimentum dolor, quis vehicula tortor hendrerit sed. Class aptent taciti sociosqu ad litora torquent per conubia nostra, per inceptos himenaeos. Etiam interdum tristique diam eu blandit. Donec in lacinia libero.

Sed elit massa, eleifend non sodales a, commodo ut felis. Sed id pretium felis. Vestibulum et turpis vitae quam aliquam convallis. Sed id ligula eu nulla ultrices tempus. Phasellus mattis erat quis metus dignissim malesuada. Nulla tincidunt quam volutpat nibh facilisis euismod. Cras vel auctor neque. Nam quis diam risus.

Nunc semper quam et leo interdum vulputate eu quis magna. Sed nec arcu at orci egestas convallis. Aenean quam velit, aliquam vitae viverra in, elementum vel elit. Nunc suscipit aliquet sapien a suscipit. Cras nulla ipsum, posuere eu fringilla sit amet, dapibus ultricies nulla. Nullam eu augue id purus mollis dignissim sed et libero. Phasellus eget justo sed neque pellentesque egestas nec id arcu. Donec facilisis pulvinar sapien et fringilla. Suspendisse vestibulum rhoncus sapien id laoreet. Morbi et orci vitae tortor imperdiet imperdiet. In hac habitasse platea dictumst. Vivamus vel neque id mi ultrices tristique. Integer quam libero, ornare vel gravida in, feugiat a ante. Nam dapibus, tellus vitae pellentesque cursus, dui nisl egestas augue, non fermentum nisl est is nec nisi. Vestibulum nec mi justo, eget dapibus velit.
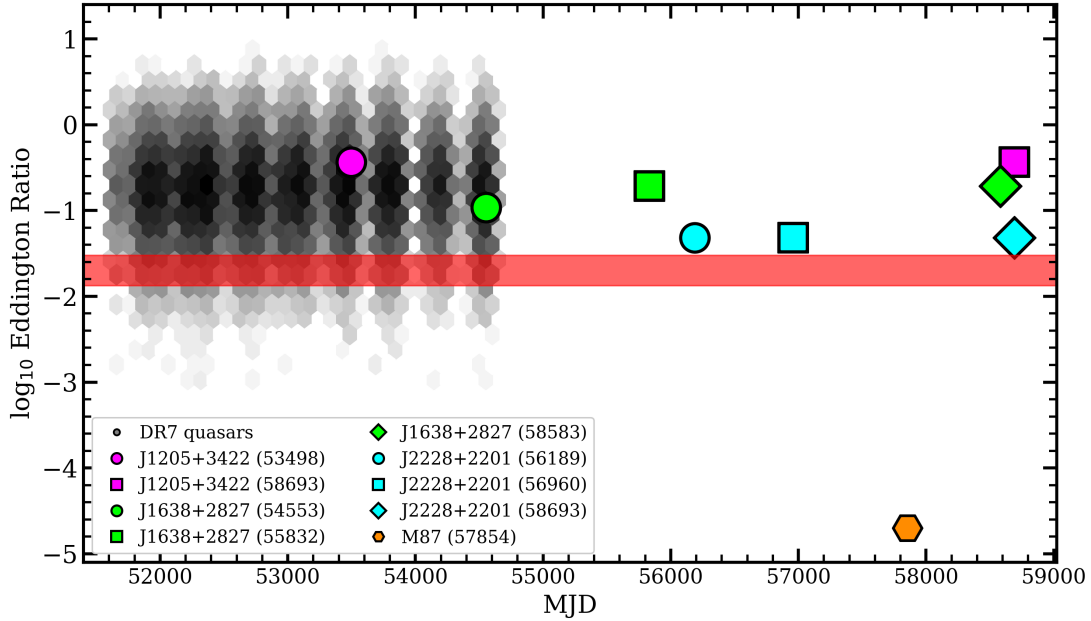
Figure 6. Eddington Ratios of the three C IV CLQs and M87.

5 CONCLUSIONS

In this paper we have reported on three redshift $z > 2$ quasars with dramatic changes in their C IV emission lines, the first 'Changing-Look' quasars at high redshift. This is also the first time the changing-look behaviour has been seen in a high-ionization emission line.

• SDSS J1205+3422, J1638+2827 and J2228+2201 show interesting behaviour in their observed optical light curves, and subsequent spectroscopy shows significant changes in the C IV broad emission line, with both line collapse and emergence being displayed in rest-frame timescales of ∼240-1640 days.

• Where observed, the profile of the Lyα/N V emission complex also changes, and there is tentative evidence for changes in the Mg II line.

• Although line measurements from the three quasars show large changes in the C IV line flux-line width plane, the quasars are not seen to be outliers when considered against the full $z > 2$ quasar population in terms of (rest) Equivalent Width and FWHM properties.

• We put these observations in context with recent "state-change" models, but note that even in their 'low-state', the C IV CLQs are above ∼ 10% in Eddington luminosity.

Etiam mollis viverra nisi eget aliquet. Aliquam erat volutpat. Vivamus tristique, nisl eu malesuada semper, libero tortor convallis elit, a scelerisque orci nisi lacinia turpis. In lacinia ultrices volutpat. Proin ultrices luctus tellus, in placerat eros tincidunt id. Ut varius iaculis quam in consequat. Nulla nec orci est, sit amet Aliquam ac metus nec odio tempus pharetra sed nec diam. Sed eget arcu nulla. Etiam elementum ultrices ligula, at iaculis libero feugiat bibendum. Suspendisse potenti. Nam pharetra adipiscing euismod. Quisque imperdiet dignissim odio, sed volutpat justo tincidunt eu. Nunc vehicula pharetra suscipit. Integer aliquet pretium ipsum vel ultrices. Nam rutrum nibh ac quam pulvinar molestie.

Availability of Data and computer analysis codes

All materials, databases, data tables and code are fully available at: `https://github.com/d80b2t/CIV_CLQs`.

University of Tokyo, University of Utah, Vanderbilt University, University of Virginia, University of Washington, and Yale University.

REFERENCES

Abazajian K. N., et al., 2009a, ApJS, 182, 543

Abazajian K. N., et al., 2009b, ApJS, 182, 543

Abolfathi et al., 2018, ApJS, 235, 42

Abramowicz M. A., Czerny B., Lasota J. P., Szuszkiewicz E., 1988, ApJ, 332, 646

Alam S., et al., 2015, preprint, (arXiv:1501.00963)

Alloin D., Pelat D., Phillips M., Whittle M., 1985, ApJ, 288, 205

Antonucci R., 2018, Nature Astronomy, 2, 504

Astropy Collaboration et al., 2013, Astron. & Astrophys., 558, A33

Bachev R., Marziani P., Sulentic J. W., Zamanov R., Calvani M., Dultzin-Hacyan D., 2004, ApJ, 617, 171

Baldwin J. A., 1977, ApJ, 214, 679

Bellm E. C., et al., 2019a, PASP, 131, 018002

Bellm E. C., et al., 2019b, PASP, 131, 068003

Bian W.-H., Fang L.-L., Huang K.-L., Wang J.-M., 2012, MNRAS, 427, 2881

Calderone G., et al., 2017, MNRAS, 472, 4051

Cutri R. M., et al., 2011, Technical report, Explanatory Supplement to the WISE Preliminary Data Release Products

Davidson K., Netzer H., 1979, Reviews of Modern Physics, 51, 715

Dawson K., et al., 2013, AJ, 145, 10

Dawson K. S., Kneib J.-P., et al., 2016, AJ, 151, 44

Dexter J., Agol E., 2011, ApJ Lett., 727, L24

Doan A. N., et al., 2019, in American Astronomical Society Meeting Abstracts #233. p. 242.23

Drake A. J., et al., 2009, ApJ, 696, 870

Drake A. J., et al., 2013, ApJ, 763, 32

Dyer J. C., Dawson K. S., du Mas des Bourboux H., Vivek M., Bizyaev D., Oravetz A., Pan K., Schneider D. P., 2019, ApJ, 880, 78

Eisenstein D. J., Weinberg D. H., et al., 2011, AJ, 142, 72

Elvis M., 2000, ApJ, 545, 63

Fukugita M., Ichikawa T., Gunn J. E., Doi M., Shimasaku K., Schneider D. P., 1996, AJ, 111, 1748

Ge X., Bian W.-H., Jiang X.-L., Liu W.-S., Wang X.-F., 2016, MNRAS, 462, 966

Graham M. J., Djorgovski S. G., Drake A. J., Mahabal A. A., Chang M., Stern D., Donalek C., Glikman E., 2014, MNRAS, 439, 703

Graham M. J., et al., 2015a, MNRAS, 453, 1562

Graham M. J., et al., 2015b, Nat, 518, 74

Graham M. J., Djorgovski S. G., Drake A. J., Stern D., Mahabal A. A., Glikman E., Larson S., Christensen E., 2017, MNRAS, 470, 4112

Graham M. J., et al., 2019a, arXiv e-prints, p. arXiv:1905.02262

Graham M. J., et al., 2019b, PASP, 131, 078001

Guo H., Sun M., Liu X., Wang T., Kong M., Wang S., Sheng Z., He Z., 2019, ApJ Lett., 883, L44

Hamann F., Ferland G., 1999, ARA&A, 37, 487

Hamann F., et al., 2017, MNRAS, 464, 3431

Hemler Z. S., et al., 2019, ApJ, 872, 21

Homan D., Macleod C. L., Lawrence A., Ross N. P., Bruce A., 2019, arXiv e-prints, p. arXiv:1910.11364

Iwasawa K., Taniguchi Y., 1993, ApJ Lett., 413, L15

Jensen T. W., et al., 2016, ApJ, 833, 199

Jiang Y.-F., Stone J. M., Davis S. W., 2014, ApJ, 796, 106

Jiang Y.-F., Davis S. W., Stone J. M., 2016, ApJ, 827, 10

Jiang Y.-F., Blaes O., Stone J., Davis S. W., 2019a, arXiv e-prints, p. arXiv:1904.01674v1

Jiang Y.-F., Stone J. M., Davis S. W., 2019b, ApJ, 880, 67

Kaiser N., et al., 2010, in Society of Photo-Optical Instrumentation Engineers (SPIE). p. 0, doi:10.1117/12.859188

Kozłowski S., 2017, ApJS, 228, 9

Kramida A., Ralchenko Y., Reader J., NIST ASD Team 2018, doi:10.18434/T4W30F,

Kramida A., Yu. Ralchenko Reader J., and NIST ASD Team 2019, NIST Atomic Spectra Database (ver. 5.7.1), [Online]. Available: https://physics.nist.gov/asd [2019, November 7]. National Institute of Standards and Technology, Gaithersburg, MD.

LaMassa S. M., et al., 2015, ApJ, 800, 144

Lawrence A., 2018, Nature Astronomy, 2, 102

Leighly K. M., 2004, ApJ, 611, 125

MacLeod C. L., et al., 2012, ApJ, 753, 106

MacLeod C. L., et al., 2019, ApJ, 874, 8

Magnier E. A., et al., 2013, ApJS, 205, 20

Mahabal A. A., et al., 2011, Bulletin of the Astronomical Society of India, 39, 387

Mainzer A., et al., 2011, ApJ, 731, 53

Masci F. J., et al., 2019, PASP, 131, 018003

Matthews T. A., Sandage A. R., 1963, ApJ, 138, 30

Meyer R. A., Bosman S. E. I., Ellis R. S., 2019, arXiv e-prints,

Murray N., Chiang J., Grossman S. A., Voit G. M., 1995, ApJ, 451, 498

Myers A. D., et al., 2015, ApJS, 221, 27

Noda H., Done C., 2018, MNRAS, 480, 3898

Oke J. B., Gunn J. E., 1983, ApJ, 266, 713

Oke J. B., et al., 1995, PASP, 107, 375

Pâris I., Petitjean P., Ross N. P., et al., 2017, Astron. & Astrophys., 597, A79

Pâris I., et al., 2018, Astron. & Astrophys.

Perrotta S., Hamann F., Zakamska N. L., Alexand roff R. M., Rupke D., Wylezalek D., 2019, MNRAS, 488, 4126

Pogge R. W., Peterson B. M., 1992, AJ, 103, 1084

Proga D., Stone J. M., Kallman T. R., 2000, ApJ, 543, 686

Rakić N., La Mura G., Ilić D., Shapovalova A. I., Kollatschny W., Rafanelli P., Popović L. Č., 2017, Astron. & Astrophys., 603, A49

Richards G. T., et al., 2002, AJ, 123, 2945

Richards G. T., et al., 2006, ApJS, 166, 470

Richards G. T., et al., 2011, AJ, 141, 167

Ross N. P., et al., 2012, ApJS, 199, 3

Ross N. P., et al., 2015, MNRAS, 453, 3932

Ross N. P., et al., 2018, MNRAS, 480, 4468

Ruan J. J., Anderson S. F., Eracleous M., Green P. J., Haggard D., MacLeod C. L., Runnoe J. C., Sobolewska M. A., 2019, arXiv e-prints, p. arXiv:1903.02553v1

Schneider D. P., et al., 2007, AJ, 134, 102

Schneider D. P., et al., 2010, AJ, 139, 2360

Seaton M. J., 1959a, MNRAS, 119, 81

Seaton M. J., 1959b, MNRAS, 119, 90

Shakura N. I., Sunyaev R. A., 1973, Astron. & Astrophys., 24, 337

Shen Y., et al., 2011, ApJS, 194, 45

Shen Y., et al., 2015, ApJS, 216, 4

Shen Y., et al., 2019, ApJS, 241, 34

Shields J. C., 2007, in Ho L. C., Wang J. W., eds, Astronomical Society of the Pacific Conference Series Vol. 373, The Central Engine of Active Galactic Nuclei. p. 355 (arXiv:astro-ph/0612613)

Smee S. A., et al., 2013, AJ, 146, 32

Stern D., et al., 2018, ApJ, submitted

Stoughton C., et al., 2002, AJ, 123, 485

Stubbs C. W., et al., 2010, ApJS, 191, 376

Sun M., Xue Y., Richards G. T., Trump J. R., Shen Y., Brandt W. N., Schneider D. P., 2018, ApJ, 854, 128

Taylor M. B., 2005, in Shopbell P., Britton M., Ebert R., eds, Astronomical Society of the Pacific Conference Series Vol. 347, Astronomical Data Analysis Software and Systems XIV. p. 29

Taylor M., 2011, TOPCAT: Tool for OPerations on Catalogues And Tables, Astrophysics Source Code Library (ascl:1101.010)

The Astropy Collaboration et al., 2018, preprint, (arXiv:1801.02634v2)

Tonry J. L., et al., 2012, ApJ, 750, 99

Vestergaard M., Peterson B. M., 2006, ApJ, 641, 689

Wilhite B. C., Vanden Berk D. E., Brunner R. J., Brinkmann J. V., 2006, ApJ, 641, 78

Wright E. L., et al., 2010, AJ, 140, 1868

York D. G., et al., 2000, AJ, 120, 1579

Zakamska N. L., et al., 2016, MNRAS, 459, 3144

Zakamska N. L., et al., 2019, MNRAS, 489, 497

This paper has been typeset from a TEX/LATEX file prepared by the author.